RSC Advances

ROYAL SOCIETY OF CHEMISTRY

www.rsc.org/advances

Synthesis, X-ray Structure of a New Zinc(II) Coordination Polymer : Interaction With DNA, Double Stranded RNA and Elucidation of the Molecular Aspects of the Binding to Bovine Serum Albumin.

Swapan K. Jana, Saikat K. Seth, Horst Puschmann, Maidul Hossain,*and Sudipta Dalai,*

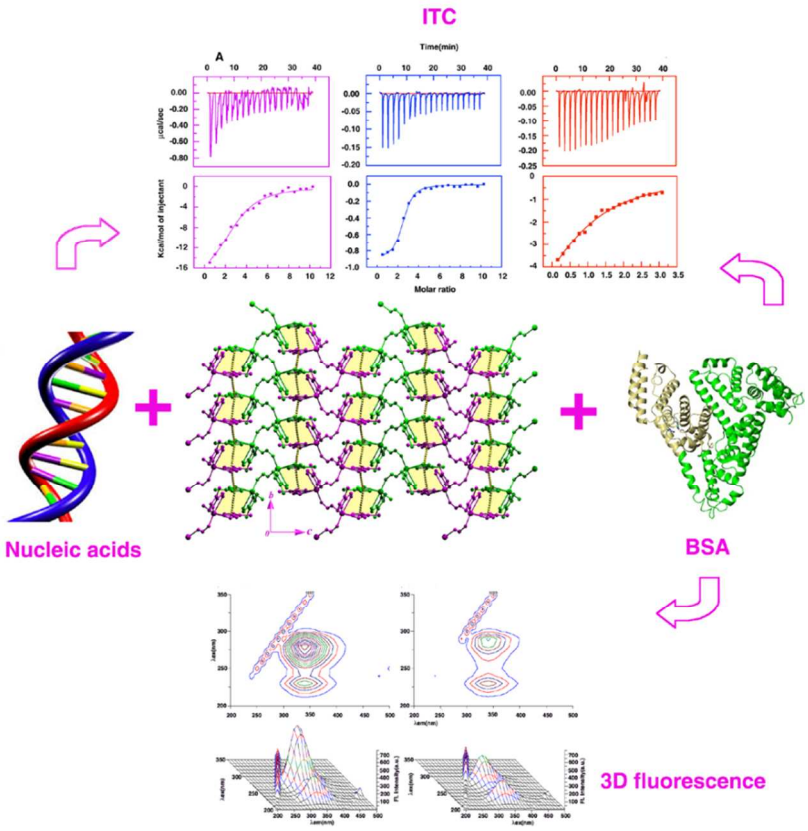

Synthesis and characterization of $[Zn(4\text{-Me-5-CHOIm})_2(HCOO)](ClO_4)$ **complex** and binding with nucleic acids and BSA has been explored by different biophysical techniques with the combination of Isothermal titration calorimetry (ITC)

Synthesis, X-ray Structure of a New Zinc(II) Coordination Polymer : Interaction With DNA, Double Stranded RNA and Elucidation of the Molecular Aspects of the Binding to Bovine Serum Albumin.

Swapan K. Jana,†,§ Saikat K. Seth,⊥ Horst Puschmann,‡ Maidul Hossain,*,†, § and Sudipta Dalai,*, †,§

† Department of Chemistry and Chemical Technology, Vidyasagar University, Midnapore 721 102, West Bengal, India.

⊥ Department of Physics, M. G. Mahavidyalaya, Bhupatinagar, Purba Medinipur, West Bengal-721425, India.

‡ Department of Chemistry, Durham University, Durham DH1 3LE, UK

■ AUTHOR INFORMATION

Corresponding Authors

*(M.H.) E-mail: hossainm@mail.vidyasagar.ac.in / maidulhossain@yahoo.com

*(S.D.) E-mail: sudipta@mail.vidyasagar.ac.in / icsdalai@gmail.com

Author Contributions

§ These authors made equal contributions.

A novel ligand bridged Zinc (II) coordination polymer, $[Zn(4\text{-Me-}5\text{-CHOIm})_2(HCOO)](ClO_4)$ has been synthesized and characterized by single crystal X-ray diffraction studies. The structural analysis revealed that the complex exhibits two types of 2D network by weak and strong hydrogen bonds. Interestingly, an extended supramolecular layer network has been observed in the solid state structure through weak face-to-face π-stacking interactions. The interaction of the complex with calf thymus DNA (CT-DNA) and double stranded ribonucleic acid, polyinosinic.polycytidylic acid (poly(I).poly(C)) has been explored by UV-Vis absorption, fluorescence displacement, circular dichroism (CD) spectral and isothermal titration calorimetric (ITC) methods. From spectral titration method revealed that compound could interact with CT-DNA and RNA through partial intercalation with a binding affinity of 10^5 orders. ITC experiments indicate an exothermic reaction in both cases but RNA interaction is favored by positive entropy. On the other hand, the complex could quench the intrinsic fluorescence of BSA in a static quenching process with quenching constant is in 10^4 order. Specific binding distance of 2.75 nm between Trp 214 (donor) and complex (acceptor) was obtained from Forster resonance energy transfer studies (FRET). Competitive binding using site markers, warfarin and ibuprofen, having definite binding sites demonstrated that complex binds to site I (subdomain IIA) on BSA. Circular dichroism (CD), synchronous fluorescence, and three-dimensional fluorescence spectroscopy experiments reveal that binding with complex, alters BSA secondary structure by a reduction of α-helical organization and increasing the coiled structure and ITC experiment indicate binding was enthalpy driven with a slight negative entropy effect.

Introduction

Small molecules interact with nucleic acid has been an active area of interest because of direct correlations of the binding to many biological activities. The interaction of small molecules to

nucleic acid can be classified in a variety of ways. But the most important are irreversible covalent and reversible non-covalent interaction. Non-covalent interactions can be further classified in terms of intercalation, groove binding and outside binding. Among the different types of DNA binding compounds, intercalating and groove binding compounds are the most widely studied as they form an important class of compounds for cancer chemotherapy[1-4]. Recently, in order to overcome toxicity and drug-resistance phenomena[5-9] and to achieve higher activity and better selectivity than platinum based anticancer drugs there is a great attention on the binding of transition metal complexes with nucleic acids[10-13]. Transition metal complexes can exhibit well-defined various geometries, coordination numbers, various oxidation states, better solubility properties, various substitution kinetics or mechanism pathways and distinctive electrochemical or photophysical properties which enhancing the functionality of the binding agent and may stimulate a pharmacological profile different than those of platinum-drugs[14-16].

Simultaneously, Serum albumins have also attracted enormous research interest as a prime molecular target[17]. Serum albumins such as bovine serum albumin (BSA) is the most multifunctional transport and distribution proteins present in plasma that can reversibly bound and carries several endo- and exo-genous compounds including proteins and fatty acids to specific targets[18,19]. It is essential to explore drug–protein interactions as most of the drugs bound to serum albumin are usually transported as a protein complex. A number of studies on the interaction of Zinc-complex to BSA have been recently undertaken[20-23] and elucidation of the molecular aspects of the binding continues to be of great importance from the stand point of understanding protein structure function on drug therapy and design.

Zinc being an essential trace element and one of the second most bio-relevant transition metal ions tends to be tightly bound within over 3000 metalloenzymes[24]. However, despite the variety

of biological activity of the zinc(II)[25-27] ion there are several reports for the utilization of the zinc complex. It is mainly utilized for the treatment of Alzheimer disease[28,29] and can act as radioprotective agents[30], tumor photosensitizers[31] anticonvulsant[32,33], antidiabetic insulin-mimetic[34-36], anti-inflammatory[37,38] , antiproliferative–antitumor[39] agents and show cytotoxicity against human cancer cell lines[40,41]. After all the binding of zinc(II) complexes to nucleic acids has attracted much attention[42-44] owing to their possible applications as new cancer therapeutic agents.

From the ligand point of view, imidazole moiety plays an important role in biological systems and variety of biologically important molecules, including the iron-heme systems, vitamin B12, histidine, biotin, etc. and their derivative shows antiinflammatory, anticancer, appetite stimulant, antitumor and antifungal activity[45-48].

Taking into consideration of biological role and the activity of zinc and imidazole moiety, herein, we report the synthesis and crystal structure of $[Zn(4\text{-Me-5-CHOIm})_2(HCOO)](ClO_4)$ coordination polymer and to explore it's as drug, in the general context of the research of potential metallodrugs**.** A thorough review of the literature has not revealed any studies concerning the interaction with DNA/RNA/BSA of the complex. Therefore, the ability of the complex to bind to calf-thymus DNA (CT- DNA) and double stranded RNA (poly(I).poly(C)) has been investigated by (i) UV spectroscopic titration studies to determine binding affinity, (ii) the competitive binding studies with ethidium bromide (EB) performed by fluorescence spectroscopy in order to investigate the existence of a potential intercalation of the complexes to DNA/RNA, (iii) circular dichroic (CD) spectral changes in order to correlate binding with structural changes (iv) thermodynamic changes associated with the binding is characterized through isothermal titration calorimetry (ITC). Furthermore, in order to understand the

transportation of the Zn(II) complex at molecular level, we also studied the interaction of the complexes with bovine serum albumin (BSA) and the binding property to BSA and thermodynamic changes associated with the binding is characterized in details, including binding domain and determination of the association constant through isothermal titration calorimetry (ITC) in combination with multiple spectroscopic techniques and two site marker probe warfarine and ibuprofen displacement methods. Structural alterations of BSA upon complexation with Zn complex are studied by synchronous fluorescence, circular dichroism (CD), and three-dimensional fluorescence techniques (3D).

Experimental section

Materials. Calf thymus (CT) DNA, Double stranded RNA polynucleotides, polyinosinic.polycytidylic acid (poly(I).poly(C)), Bovine serum albumin (BSA), warfarin, ibuprofen, EB was obtained from Sigma-Aldrich Chemicals Co., (St. Louis, MO, USA) and used as received without further purification.. Concentration of Calf thymus DNA was determined spectrophotometrically using a molar extinction coefficient (ε) 13,200 (M^{-1} cm^{-1}) at 260 nm and 10,000 M^{-1} cm^{-1} at 260 nm for poly(I).poly(C) expressed in terms of molarity of base pairs throughout. The concentration of BSA, warfarine, ibuprofen were determined using molar extinction coefficients values 43,824 M^{-1} cm^{-1} at 280 nm for BSA, 13,900 M^{-1} cm^{-1} at 308 nm and 346 M^{-1} cm^{-1} at 272 nm for warfarine and ibuprofen respectively. No deviation from Beers law was observed in the concentration range employed in this study.

All experiments were conducted in citrate-phosphate (CP) buffer 10 mM [Na^+], pH 7.1, containing 0.5 mM Na_2HPO_4. The pH was adjusted by addition of citric acid. Quartz distilled deionized water and analytical grade reagents were used throughout. All buffer solutions were passed through Millipore filters of 0.45 μm (Millipore India Pvt. Ltd., Bangalore, India) to

remove any particulate matter. 4-Me-5-CHOIm was purchased from Sigma-Aldrich. The reagents perchloric acid and formic acid were purchased from Merck. All the chemicals and solvents were used without further purification.

Caution! Perchlorate salt of metal complex with organic ligands is potentially explosive. Only a small amount of material should be prepared, and it should be handled with care.

Synthesis of [Zn(4-Me-5-CHOIm)$_2$(HCOO)](ClO$_4$) Complex.

4-Me-5-CHOIm (1 mmol, 0.110 g) was dissolved in 10 ml methanol. To this solution, 5 ml methanolic solution of $Zn(ClO_4)_2.6H_2O$ (0.5 mmol, 0.186 g) was added drop wise with continuous stirring. After 30 m, formic acid (0.5 mmol, 19.25 µl) was added to the solution. The resulting mixture was stirred for 2 h to get a transparent yellow solution. The solution was kept in dark for crystallization. After seven days diffraction quality plate like light yellow single crystals were obtained by slow evaporation of the solvent. Yield 70%. Anal. Calcd. for $ZnC_{11}H_{13}O_8N_4Cl$: C, 30.72; H, 3.04;N, 13.02%.Found: C, 30.81; H, 3.03; N, 12.98 %.IR (KBr, cm^{-1}): 548 (w), 625 (m), 686 (m), 779 (m), 817 (m), 983 (m), 1071 (m), 1156 (w), 1245 (m), 1318 (m), 1360 (m), 1414 (w), 1549 (w), 1641 (s).

Crystallographic analysis.

Single crystal X-ray diffraction intensity data of the title complexes were collected at 293(2)K using a Bruker APEX-II CCD diffractometer equipped with graphite monochromated M_oK_α radiation (λ=0.71073Å). Data reduction was carried out using the program Bruker SAINT[49]. An absorption correction based on multi-scan method[50] was applied. The structures were solved by direct methods and refined by the full-matrix least-square technique on F^2 using the programs SHELXS97 and SHELXL97[51] respectively. All calculations were carried out using WinGX system Ver-1.64[52] and PLATON[53]. All hydrogen atoms were located from difference Fourier map and treated as riding. A summary of crystal data and relevant refinement

parameters are given in Table 1. CCDC deposition No. 979508 contains the supplementary crystallographic data for this paper. The data can be obtained free of charge via http://www.ccdc.cam.ac.uk/conts/retrievinghtml (or from the CCDC, 12 Union Road, Cambridge CB2 1EZ, U.K.; Fax: +44−1223−336033; E-mail: deposit@ccdc.cam.ac.uk).

Equipments and spectral measurements.

Infrared spectra of the metal complex were recorded in the range of 3000–500 cm^{-1} using a Perkin Elmer Spectrum two FT-IR spectrophotometer from KBr discs.

NMR spectra of the D_2O solutions (294 K) of the Zn(II) complexes were taken on a Bruker- 400 spectrometer and were recorded at 400.0 MHz.

A Shimadzu Pharmaspec 1601 unit (Shimadzu Corporation, Kyoto, Japan) was used for absorption spectral studies where a constant concentration of the complex was treated with increasing concentration of DNA/RNA in one cm path length matched quartz cells with continuous stirring throughout the course of the titration. While measuring the absorption spectra, an equal amount of DNA/RNA was added to both the test solution and the reference solution to eliminate the absorbance of DNA/RNA itself. From the absorption titration the intrinsic binding constant K_b was calculated from the following equation[54]

$$\frac{[Nucleic\ acid]}{(\varepsilon_a-\varepsilon_f)} = \frac{[Nucleic\ acid]}{(\varepsilon_b-\varepsilon_f)} + \frac{1}{K_b(\varepsilon_b-\varepsilon_f)} \qquad \text{……..(1)}$$

Where [Nucleic acid] is the concentration of DNA/RNA in the base pairs, ε_a is the apparent absorption coefficient corresponding to A_{obs}/ [compound], ε_f is the extinction coefficient of the free compound, and ε_b is the extinction coefficient of the compound when fully bound to Nucleic

acid. From the plot of [Nucleic acid]/($\varepsilon_a - \varepsilon_f$) versus [Nucleic acid] , the intrinsic binding constant K_b can be calculated by the ratio of the slope to intercept.

Fluorescence spectral studies were performed on a Hitachi F7000 (Hitachi Ltd., Tokyo, Japan). Competitive binding studies of the complex with ethidium bromide (EB) have been performed to examine whether the compound can displace EB from its CT-DNA/RNA–EB complex by fluorescence spectroscopy. The CT- DNA/RNA–EB complex was prepared by adding 5 μM EB and 15 μM CT- DNA/RNA in 10mM [Na+] CP buffer (pH 7.1). The CT-DNA/RNA –EB complex was excited at 515 nm, and the emission range was recorded at 530–700 nm. The fluorescence intensities were recorded by adding a certain amount of a solution of the compound step by step into the solution of the CT-DNA/RNA–EB complex.

The fluorescence quenching of the proteins was measured by an excitation wavelength of 295 nm keeping excitation and emission band passes of 5 nm because it is exclusively due to the intrinsic tryptophan (Trp) fluorophore. Synchronous fluorescence was measured in the excitation range of 220–340 nm keeping $\Delta\lambda$ set at 15 and 60 nm. Three-dimensional fluorescence spectroscopy experiments were performed using initial wavelength was set at 200 nm and continued up to 350 nm with an increment of 10 nm for each scan. The fluorescence emission spectra of BSA were measured in the range of 200-500 nm. The concentration of BSA was 2.5 μM and the BSA–complex ratio was 1 : 10.

All the isothermal titration calorimetry (ITC) experiments were performed on a GE Microcal ITC 200, (Northampton, USA) microcalorimeter. Origin 7.0 software was used for data acquisition and manipulation. In typical experiment aliquots of degassed DNA/RNA/BSA solution were injected from a rotating syringe (750 rpm) into the isothermal sample chamber containing the complex solution. Corresponding control experiments to determine the heat of

dilution of DNA/RNA/BSA were performed by injecting identical volumes of DNA/RNA into the buffer. The volume of the injection was 2µl and duration of each injection was 4 s and the delay time between each injection was 120 s. The initial delay before the first injection was 60 s. Each injection generated a heat burst curve (micro calories per second versus time). The area under each heat burst curve was determined by integration using the Origin 7.0 software (MicroCal) to give the measure of the heat associated with that injection. The heat associated with each DNA/RNA/BSA-buffer mixing was subtracted from the corresponding heat associated with the DNA injection to the complex to give the heat of complex binding to DNA/RNA/BSA. The heat of dilution of injecting the buffer into the complex solution was observed to be negligible. The resulting corrected injection heats were plotted as a function of the [complex]/[molar ratio], fit with a model for one set of binding sites, and analyzed using Origin 7.0 software to estimate the binding affinity (K_b), the binding stoichiometry (N) and the enthalpy of binding (ΔH). The free energies (ΔG) were calculated using the standard equation:

$$\Delta G = -RT \ln(K_b) \quad \ldots \quad \ldots \quad \ldots \quad (2)$$

where R is 1.987 cal/ mol, K and *T* is represented in units of Kelvin for the appropriate temperature. The binding free energy coupled with the binding enthalpies derived from the ITC data allowed the calculation of the entropic contribution to the binding ($T\Delta S$), where $T\Delta S$ is the calculated binding entropy using the standard relationship,

$$T\Delta S = \Delta H - \Delta G \ldots \quad \ldots \quad \ldots \quad (3)$$

Circular dichroism (CD) spectra were recorded at 25^{o}C on a PC driven Jasco J815 spectropolarimeter (JASCO International Co. Ltd., Tokyo, Japan) attached with a Peltier controlled cell holder and temperature controller PFD 425 L/15 in rectangular quartz cuvettes of

1 cm path length for DNA/RNA and 0.1cm path length for BSA. Each spectrum was averaged from four successive accumulations at a scan rate of 100 nm/min, keeping a bandwidth of 1.0 nm at a sensitivity of 200 mdeg, and was baseline corrected and smoothed within permissible limits us*in*g the inbuilt software of the unit. A fixed concentration of DNA/RNA/BSA was titrated with increasing concentration of complex. The molar ellipticity values were expressed in terms of the mean residue molar ellipticity [θ], in units of deg cm^2 $dmol^{-1}$.

Results and discussion

Crystallography: The molecular view[55] of Zn^{II} complex is depicted in Fig. 1 with atom numbering scheme. The metal atom exhibits an elongated octahedral coordination type 4+1+1, supplied by two Im ligands, which donates two nitrogen and two oxygen atoms and two more coordination sites are supplied by the oxygen atoms of two formate anions. Thus the Zn^{II} atom exhibits a distorted octahedral ZnN_2O_4 chromophore. It is interesting to mention that the bond distances of Zn–O (Im ligands) are longer compare to the Zn–O (formate anions). In the title complex, the 4-Me-5-CHOIm ligand forms two five-membered chelate rings (Fig. 1). The structure of the complex includes a combination of N–H···O and C–H···O hydrogen bonding interactions (Table 2) along with π–π stacking interactions (Table 3). In the title complex, the methyl carbon atom C16 in the molecule at (x, y, z) acts as a donor to the oxygen atom O21 in the molecule at (2-x, 1-y, -z), so generating a centrosymmetric $R_2^2(14)$ dimeric ring (M) centred at (1, ½, 0) (Fig. 2). Additional reinforcement between these molecules which combine to form M type of dimer, is provided by a pair of C17–H17···O21 hydrogen bonds (Table 2) in the molecules at (x, y, z) and (x, 1+y, z) form a characteristic $R_4^2(14)$ ring motif (N) (Fig. S1 in the Supporting Information (SI)). Thus these two types of $R_2^2(14)$ and $R_4^2(14)$ ring motifs are alternatively linked into infinite MNMNMN…… ribbon propagating along (0 1 0) direction.

Due to the self-complementarity of the molecules, they recognize themselves to generate $R_2^2(10)$ ring motif (P) on either side of this ribbon (Fig. S1 in the Supporting Information (SI)). Interconnections of the successive ring motifs (M and N type) along the crystallographic *b*-axis define well-connected columns to form a supramolecular ribbon in which the P-type ring motif act as the node along (1 0 0) direction and are displaced sidewise with respect to the successive ribbons, thus generating a two-dimensional supramolecular framework in (1 1 0) plane (Fig. S2 in the Supporting Information (SI)). In another substructure, the nitrogen atom N23 acts as donor to the oxygen atom O1s in the molecule at (1-x, 1-y, -z) and then nitrogen atom N13 acts as double donor to the O2s and O4s in the molecule at (2-x, 1-y, -z) to generate a one dimensional chain parallel to crystallographic *a*-axis. These parallel chains which propagates along (1 0 0) direction are interlinked by another N–H···O hydrogen bonds where N23 in the molecule at (x, y, z) acting as donor to the oxygen atom O11 in the molecule at (1-x, 1-y, -z); thus generating a two-dimensional supramolecular framework in (1 0 1) plane (Fig. S3 in the Supporting Information (SI)).

Analysis of weak intermolecular interactions involved within the structure shows that the π–π stacking interactions (Table 3) plays a decisive role in building unique layered assembly. The adjacent monomeric units are packed in face-to-face orientation where the 4-Me-5-CHOIm rings (N21/C22/N23/C24/C25) are juxtaposed in the molecule at (x, y, z) and (1-x, -y, -z). These rings are strictly parallel with an interplanar spacing of 3.256Å, with a ring centroid distance of 3.469(2)Å, corresponding to a ring offset 1.198Å. The π-stacked molecular fragment is forming a layer network along (0 1 0) direction through another face-to-face stacking interaction in the molecule at (x, y, z) and (1-x, 1-y, -z), where, the intercentroid separation is 3.728(2)Å and the interplanar spacing is 3.212Å, corresponding to a ring offset of 1.892Å (Fig. S4 in the

Supporting Information (SI)). Due to self-complementarity of weak intermolecular interactions, these individual multi π-stacked layers recombine themselves to build a supramolecular layer network (Fig. S4 in the Supporting Information (SI)).

Characterization of the zinc Complex in solution: The stability of the complex was investigated by ^{1}H and ^{13}C NMR in aqueous (D_2O) solution and depicted in Fig. S5-S10 in the Supporting Information (SI). ^{1}H NMR of free 4-Me-5-CHOIm ligand shows d valued: 9.78 (s, 1H,CHO), 7.71 (s, 1H, CH), 4.75 (s, NH, H2 (residual water from D2O)), 2.40 (s, 3H, CH3) ppm (Fig. S5) and in complex shows a δ values: 9.63 (s, 1H, CHO), 7.86 (s, 1H, CH), 4.80 (s, NH, H2 (residual water from D2O)), 2.46 (s, 3H, CH3) ppm with a additional peak at 8.33(s,1H, $CH00^{-}$).On the other hand 13C NMR shows δ values: 215.39(-C*HO), 185.43(NH-C*H-N), 138.44(CHO-C*-NH), 30.28(-C*H-Me), and 9.76(-$C^{*}H_3$) ppm for ligand 4-Me-5-CHOIm (Fig. S6) and complex shows 215.40(-C*HO), 184.23(NH-C*H-N), 163.85(HC*OO-), 138.12(CHO-C*-NH), 30.25(-C*H-Me), and 22.20(-$C^{*}H_3$) ppm respectively. In presence of DNA the chemical shift values remain exatly same as in solution(Fig.S9&S10). Compearing the chemical shift value it was clear that the complex exist as $[Zn(4\text{-Me-5-CHOIm})_2(HCOO)]^{+}$ in solution. The species was also identified by ESI-MS spectra in aqueous solution (*m/z* =330) (Fig.S11) in the Supporting Information (SI).

DNA and RNA binding studies: DNA interacting agents are of exceptional importance in cancer biology due to their potential therapeutic use. A large number of currently utilized small molecule anticancer agents exert their effect by acting on DNA. Non-covalent interaction of such natural and synthetic products to DNA mostly involves either an intercalative or minor groove binding mechanism. On the other hand some DNA binding small molecules was exhibit strong affinity towards synthetic RNA. Hence the study of DNA/RNA interaction with metal complex

is essential for further development of more effective therapeutic agents. The binding mode, mechanism of the complexation to CT DNA and double stranded RNA poly(I).poly(C) was studies with different biophysical techniques.

Electronic absorption titration and binding affinity evaluation. Interaction of metal complex compounds with DNA/RNA can be conveniently monitored using electronic spectroscopy by the changes in the absorbance and the shift in the wavelength maxima. In general, the metal complexes binding to DNA/RNA through intercalation results in hypochromic and bathochromic effects in the absorption bands of the complex molecule because the intercalative mode involves in a strong stacking interaction between the planar aromatic chromophore and the base pairs of DNA/RNA. The representative absorption spectra of the complexes in the absence and presence of CT-DNA and double stranded RNA poly(I).poly(C) are shown in Fig. 2. From the absorption titration spectrum (Fig. 2) it is evident that upon addition of CT DNA and double stranded RNA poly(I).poly(C) to a solution , the intra ligand band (268 nm) displayed hyperchromism along with a negligible blue shift (~264 nm) suggesting a conformational change of the complex. The results derived from the UV titration experiments suggest that the compounds can bind to CT DNA/ double stranded RNA poly(I).poly(C). The hyperchromism observed may be a first evidence of possible external binding , while the existence of a blue shift for 2nm may suggest stabilization upon binding to DNA/RNA; in such case, intercalation due to $\pi \rightarrow \pi^*$ stacking interactions between the base pairs of CT DNA/ double stranded RNA poly(I).poly(C) may not be ruled out[20,56,57]. Nevertheless, the exact mode of binding cannot be simply proposed by UV spectroscopic titration studies. The binding constant of the compounds to CT DNA and double stranded RNA poly(I).poly(C) (K_b) is obtained by the ratio of the slope to the y intercept in plots $([DNA][RNA])/(\varepsilon_a - \varepsilon_f)$ versus [DNA]/RNA according to equation (1). The solid lines in the

inset of Fig. 6 represent the best fit of the experimental value to equation (1). The remarkable result that emerged from this experiment and analysis was that complex bind to CT- DNA and double stranded RNA poly(I).poly(C) with an intrinsic binding affinity (K_b) of (1.02± 0.10)x10^5 M^{-1} and (1.26 ± 0.20) × 10^5 M^{-1} respectively. Same experiment done with free ligand but there was negligible change in the absorption band (Fig.S12 in the Supporting Information (SI)) indicates a very weak interaction. Tarushi et.al. reported that [Zn(flmq)$_2$(phen)] , [Zn(oxo)$_2$(bipy)] have the binding constant (2.02±0.21)×10^6 and (6.25±0.15)×10^4 M^{-1} respectively and suggested a high to moderate binding[58]. Arjmand et.al. showed the binding constant of [Zn(II).Val-Pro], [Zn(II).Ala-Pro] towards DNA were 1.90 ×10^4 and 9.90 × 10^3 M^{-1} conclude a groove binding[57]. Zianna et.al shows that the binding affinities of [Zn(5-NO2-salo)$_2$(phen)], [Zn(5-NO2-salo)$_2$(dpamH)], [Zn(5-Cl-salo)$_2$(bipy)], [Zn(5-Cl-salo)$_2$(dpamH)], [Zn(5-Br-salo)$_2$(bipy)], [Zn(5-Br-salo)$_2$(phen)], [Zn(5-Br-salo)$_2$(dpamH)] towards CT DNA were between (1.75±0.17) × 10^4 and (8.78±0.35) × 10^5 M^{-1} and suggest a strong binding[59]. Giannicchi et al. investigate the binding of Zn- salophen complexes to CT DNA and calculate the binding between 8.8x10^4 to 1.5 × 10^5 M^{-1} and more recently Mrkalić et.al. estimate a number of binding constant such as [Zn(bpo)$_2$(H_2O)$_2$] , [Zn(bpo)$_2$(bipy)], [Zn(bpo)$_2$(phen)] and [Zn(bpo)$_2$(dpamH)] to CT DNA between (6.06±0.22) × 10^4 and 7.68(±0.16) × 10^5 M^{-1} and suggest strong binding[60,61].In this study calculated K_b values for the compound suggest a strong binding to CT DNA and RNA although slightly high binding for RNA.

Ethidium Bromide (EB) displacement studies. Absorption spectral studies shows that the strong binding of the complex with CT-DNA/ double stranded RNA poly(I).poly(C). To confirm the binding mode, EB displacement experiments have been performed. EB is a planar, cationic dye, and it is generally used as a sensitive fluorescence probe for DNA. EB has no or marginal

fluorescence but in presence of DNA/ double stranded RNA poly(I).poly(C) due to its strong intercalation between the adjacent DNA base pairs show highly fluorescent behavior[62,63]. Therefore, the EB displacement technique can provide indirect evidence for the DNA binding mode[64-67]. The displacement technique is based on the decrease of fluorescence resulting from the displacement of EB from a DNA /RNA by a quencher, and the quenching is due to the reduction of the number of binding sites on the DNA/RNA that is available to the EB. The emission spectra of the DNA–EB/RNA-EB system with increasing the concentration of the Zn(II) complexes are shown in Fig.S13 in the Supporting Information (SI). An increase in the concentration of complex leads to hypochromism with red shift relative to initial fluorescence intensity. It suggested that EB molecules are displaced from the DNA/RNA binding sites by complex under investigation. Quenching parameters were analyzed following the Stern–Volmer equation.

$$\frac{F^0}{F} = K_{SV}[Q] + 1 \qquad \text{.....(4)}$$

Where F^0 is the emission intensity in the absence of compound, F is the emission intensity in the presence of compound, K_{SV} is the quenching constant, and [Q] is the concentration of the compound. The K_{SV} value is obtained as a slope from the plot of F^0/F versus [Q]. Further, the apparent DNA/RNA binding constant (K_{app}) values were also calculated using the following equation

$$K_{EB}[EB] = K_{app}[complex]$$

where, [complex] is the value at 50% decrease in the fluorescence intensity of CTDNA- EB / double stranded RNA poly(I).poly(C) -EB complex, $K_{EB}(11.30 \pm 0.72 \times 10^6\ M^{-1})$, $(5.19 \pm 0.12 \times 10^6\ M^{-1})$ are the DNA and RNA binding constant of EB respectively, and [EB] is the

concentration of EB (5 μM). The K_{SV} value for complex was found to be 2.47×10^3 M^{-1} for DNA and 2.20×10^3 M^{-1} RNA respectively with a K_{app} value 6.78×10^5 M^{-1} and 3.16×10^5 M^{-1}. Tarushi et.al. reported that [Zn(flmq)$_2$(phen)] , [Zn(oxo)$_2$(bipy)] have the K_{SV} value $(1.54\pm0.01)\times10^5$ and $(4.60\pm0.19)\times10^5 M^{-1}$ respectively and suggested a intercalative mode[58]. Zianna et.al shows that the K_{SV} value of [Zn(5-NO2-salo)$_2$(phen)], [Zn(5-NO2-salo)$_2$(dpamH)], [Zn(5-Cl-salo)$_2$(bipy)], [Zn(5-Cl-salo)$_2$(dpamH)], [Zn(5-Br-salo)$_2$(bipy)], [Zn(5-Br-salo)$_2$(phen)], [Zn(5-Br-salo)$_2$(dpamH)] towards CT DNA-EB displacement were between$(1.45\pm0.02) \times 10^4$ to $(5.59\pm0.18) \times 10^5$ M^{-1} and suggest a strong intercalation binding mode[59]. Giannicchi et al. investigate the binding of Zn- salophen complexes to CT DNA and calculate the K_{SV} value $9.4x10^3$ M^{-1} and more recently Mrkalić et.al. estimate a number of K_{SV} value constant such as [Zn(bpo)$_2$(H$_2$O)$_2$] , [Zn(bpo)$_2$(bipy)], [Zn(bpo)$_2$(phen)] and [Zn(bpo)$_2$(dpamH)] to CT DNA between $(7.63\pm0.26) \times 10^4$ and $(4.90\pm0.15) \times 10^5$ M^{-1} suggesting a intercalation mode[60,61.] From the observed quenching and binding parameters we conclude that the complex bind DNA via weak intercalation mode[68-70]

Circular Dichroism (CD) studies. Circular dichroic spectral studies provide good evidence for conformational change of the CT-DNA/ double stranded RNA poly(I).poly(C) structure on the interaction of the complex .The CD spectra monitors the asymmetric environment of the complex when bound to DNA/RNA and therefore can be used to obtain information on the binding mode particularly since the complex is optically inactive molecule. The right-handed B form CT-DNA exhibits two characteristic CD bands, a positive band at 275 nm due to base stacking and a negative band at 248 nm due to right handed helicity while poly(I)poly(C) shows two well-defined bands with maxima at 243 and 276 nm, and a minimum at 262 nm. These bands are sensitive towards binding of any small molecule and therefore it is useful to

monitoring these bands for the conformational changes occur of DNA/RNA in presence of complex. The intrinsic CD of the DNA- complex and RNA-complex is presented in Fig. 3. The increase in concentration of complex produced moderate increase in the positive (275 nm) and negative CD (248 nm) bands of the B-from CD of CT-DNA (Fig. 3A). The binding of classical intercalators produced reasonable increment in the in the positive (275 nm) and negative CD (248 nm) bands of the B-from DNA due to the lengthening of the helix and the weakening of the base stacking interactions[71]. On the other hand circular dichroic spectral results shown in Fig. 3B reveal that the conformation of poly(I)poly(C) has been remarkably altered by the binding of complex. The moderate decrease in the CD signal at 278nm and 243nm region clearly suggested the alteration of the poly(I)poly(C) secondary structure on binding of complex[72,73]. Chu et al shows that Zn(II) complexes with 4'-(4-(2-(piperidin-1-yl)ethoxy)phenyl)-2,2':6',2"-terpyridine Interact with DNA and give both positive and negative signal increase moderately and suggest a weak intercalating mode[74]. Similar result was shown by Nakamura et al with [Zn(II)(phen)(edda)] and suggested a weak intercalation mode[75]. In our studies we found that moderate increase in intensity of both band of CT-DNA and the moderate decrease in the ellipticity of the bands, particularly the long wavelength band of poly(I)poly(C) has been correlated to the function of both helix winding angle and base pair twist which may indicate a weak intercalation mode. These results show good agreement with EB displacement study.

***Isothermal titration calorimetric studies*.** Isothermal titration calorimetry has become an important tool for direct and reliable measurement of the thermodynamic parameters of the interaction of small molecules to DNA[76]. The thermodynamic parameters like Gibbs energy change (ΔG), enthalpy of binding (ΔH), the entropy contribution ($T\Delta S$), the affinity (K_b) and stoichiometry (N) directly obtained from this experiment. The representative calorimetric profile

of the titration of the complex with DNA/RNA is presented in Fig.4A&B and the resulting binding parameters are depicted in Table 4. It can be seen that binding of complex to DNA /RNAgive ITC thermograms consistent with exothermic binding. The titration experiment of complex to DNA/RNA showed a single exothermic event. The calorimetric data were fitted to a single set of identical sited model yielding a ΔH = -53.69±1.90 kcal mol^{-1}, a stoichiometry (N) of 0.359 and K_b = (1.8 ± 0.39) x 10^5 M^{-1} and the entropy contribution ($T\Delta S$) = -46.51kcal/mole for CT –DNA while Kb=(2.81 ± 0.17) x 10^5 M^{-1}, an enthalpy ΔH= -3.09 ± 0.03 kcal.mol^{-1}, an entropy change $T\Delta S$= 4.35 kcal.mol^{-1} and a binding site size (N) of 0.390 base pairs for poly(I).poly(C) at 298.15K. The apparent stoichiometry values estimated around 0.359 and 0.390, the reciprocal of which is around 2.785 and 2.54 base pairs and this compares well with the values obtained from neighbour exclusion analysis. On the other hand when the $Zn(ClO_4)_2.6H_2O$ titrated with CT –DNA yield a ΔH = -0.50±0.02 kcal mol^{-1}, a stoichiometry (N) of 0.95 and K_b = (2.4 ± 0.19) x 10^4M^{-1} and the entropy contribution ($T\Delta S$) = 5.57 kcal/mole while, K_b=(4.06 ± 0.11) x 10^3 M^{-1}, an enthalpy ΔH= 1.46 ± 0.02 kcal.mol^{-1}, an entropy change $T\Delta S$= 6.38 kcal.mol^{-1} and a binding site size (N) of 1.05 base pairs for poly(I).poly(C)(Fig S14A,B and Table S2 in the Supporting Information (SI).) at 298.15K. From this comparative experiment we observed that the binding constant and other thermodynamic data are well different between complex and metal salt.

For intercalators, the magnitude of the binding enthalpy is large and negative. It is significant to observe that the association of complex to DNA /RNAwere suggested to be enthalpy driven . These values are similar to that observed for other intercalators[76].

Protein binding studies:

Absorption spectral study of the interaction. To obtain the interaction mode of quenching mechanism absorption spectral studies was performed as the quenching mechanism may follow either static or dynamic mode. Static quenching usually results from the formation of a complex between quencher and fluorophore in the ground state, whereas in dynamic quenching the fluorophore and quencher get in touch with each other during the transient existence of the excited state[77] . Careful examination of the absorption spectra of the fluorophore in presence and absence of quencher can help to distinguish static and dynamic quenching. In difference, ground-state complex formation will result in perturbation of the absorption spectrum of the fluorophore but Collisional quenching(dynamic) only affects the excited states of the fluorophores, and therefore, no changes in the absorption spectra are expected. The absorption spectra of BSA in the absence and presence of the compounds and the difference spectra between BSA-complex 1:1mixture and complex is presented in Fig. S15 in the Supporting Information (SI). Among the two peaks of BSA, the absorption peak at about 213 nm reflects the framework conformation and peak at about 279 nm appears to be due to the aromatic amino acids (Trp, Tyr, and Phe) of the protein. Absorption peak of BSA at 276nm show a hyperchromosm and shift of 2nm as the complex was added. This result clearly indicates a static interaction between BSA and the added complex reported earlier[20,70,78,79].

Fluorescence spectral study. BSA contains three types of fluorophores viz. Tryptophan (Trp), Tyrosine (Tyr) and Phenylalanine (Phe). BSA contains two tryptophan (Trp) residues that possess intrinsic fluorescence[80,81]. Trp 134 in the first domain is located on the surface in the hydrophilic region of the protein while Trp 212 in the second domain is located within a hydrophobic binding pocket. When excited at 295 nm, the fluorescence of BSA mostly comes from the Trp residue at position 212. Variation in the emission spectra arises mostly from the

tryptophan residue because of changes in protein conformation or denaturation. Hence, fluorescence behavior of BSA can provide significant information about the structure, dynamics, and protein folding. Addition of complex leads to decrease in the fluorescence intensity may be due to a variety of interactions like excited state reactions, molecular rearrangements, energy transfer, ground state complexation and collision quenching. The effects of addition of complex on the fluorescence emission spectrum of BSA are shown in Fig.5A.

The quenching data was quantified by Stern-Volmer equation

$$\frac{F^0}{F} = 1 + Kq\tau_0[Q] = 1 + K_{SV}[Q] \qquad \ldots\ldots\ldots\ldots\ldots\ldots\ldots\ldots \qquad (5)$$

where F^o and F are the fluorescence intensities in the absence and in the presence of the quencher, respectively. K_q is the quenching rate constant. K_{sv} is the dynamic quenching constant, τo is the average life time of the protein in the absence of quencher which is of the order of 10^{-8} s (5 ns)[82-84] and [Q] is the concentration of the quencher (complex). Dynamic quenching refers to a process when the fluorophore and the quencher come into contact during the life time of the excited state. Static quenching, on the other hand, refers to fluorophore-quencher complex formation. The plot of F/F_o versus [Q] showed linear plot (not shown), which is indicative of one type of quenching. The K_{sv} value obtained from this plots had values of 4.85 x 10^4 L. mol^{-1} and K_q calculated from the ratio of K_{sv} and τo showed value of 4.85 x 10^{12} L mol^{-1} s^{-1}. For dynamic quenching, the maximum value of scattering collision quenching constant, K_{diff} is 2.0 x 10^{10} L mol^{-1} s^{-1}[82-84]. Since the value of the biomolecular quenching is higher, it can be assumed that the complex formation between the quencher and the protein leading to a static mechanism.

Site selective binding of complex. To further locate whether binding of complex to BSA occurs to site I and/or II, the site marker fluorescence probes warfarin and ibuprofen were used.

Warfarin, an anticoagulant, explicitly binds to Sudlow's site I in the subdomain IIA while ibuprofen primarily binds to Sudlow's site II located in the subdomain IIIA[85-87]. Competitive binding experiments were carried out with BSA-warfarin and ibuprofen in presence of complex and the results are presented in Fig. 5B-C. The emission maximum of BSA shifts from 340 to 346 nm on complexation with warfarin (Fig. 5B). Addition of complex quenched the fluorescence intensity of BSA with a red shift of the maximum from 346 nm to around 348 nm. Fig. 9C presents the comparative competitive binding pattern of ibuprofen-BSA complex with Zn complex. By contrast with warfarin, the fluorescence intensity of ibuprofen-BSA complex was the same as that in the absence of ibuprofen and the binding of complex induced quenching as in the absence of ibuprofen indicating that binding was unaffected in presence of ibuprofen. These observations suggest that complex binds to site I in the subdomain IIA of BSA. To evaluate quantitatively the binding of complex in presence of these site markers, the binding constants in presence of them were analyzed by Stern-Volmer equation (6) and presented in Table 5.

In Fig. 5D the Stern-Volmer plots of BSA-complex complexation in presence of warfarin and ibuprofen are presented. The results reveal that the binding was only marginally affected in presence of ibuprofen while it was remarkably affected in presence of warfarin confirming the affinity of complex to Trp 212 of site I (subdomain IIA) of BSA (Table 5).

Energy transfer from BSA to complex and binding distance.

The Föster resonance energy transfer (FRET) has been employed for determining molecular distances in biological and macromolecular systems frequently[88,89]. If there is overlap between the fluorescence emission spectrum of the donor and the absorbance spectrum of the acceptor or when the distance between the donor and acceptor is <8 nm,energy transfer could occur through

direct electrodynamic interaction between excited donor molecule and its acceptor molecules[90]. The overlap of the fluorescence emission spectrum of BSA with the absorption spectrum of complex is shown in Fig. S16 in the Supporting Information (SI). According to Förster's theory[77], the efficiency of energy transfer between the donor and the acceptor, *E*, can be calculated using the equation,

$$E = 1 - \frac{F}{F_O} = \frac{R_O^6}{R_O^6 + r^6} \quad \text{...(6)}$$

where E is the efficiency of energy transfer, F and F_o are the fluorescence intensities in presence and absence of complex and, r is the binding distance between donor and acceptor, and *R*o is the critical distance when the transfer efficiency is 50%,

$$R_0^6 = 8.8 \times 10^{-25} k^2 n^{-4} \varphi J \quad \text{... (7)}$$

where k^2 is the spatial orientation factor of the dipole, *n* is the refractive index of the medium, φ is the fluorescence quantum yield of the donor, and J is the overlap integral of the fluorescence emission spectrum of the donor with the absorption spectrum of the acceptor. The value of J can be calculated by the following equation:

$$J = \frac{\int_0^\infty F(\lambda)\varepsilon(\lambda)\lambda^4 d\lambda}{\int_0^\infty F(\lambda) d\lambda} \quad \text{.. (8)}$$

where F(λ) is the fluorescence intensity of the donor at wavelength *λ* and ε(λ) is the extinction coefficient of the acceptor at *λ*. J can be evaluated by integrating the overlapping region between the donor fluorescence and acceptor absorbance as shown in Fig. S16. In the present case, k^2 = 2/3, *n* = 1.36 and *φ* = 0.015 for BSA[90,91]. From Eq. 4-6, the values of the parameters were found to be $J = 1.1902 \times 10^{-15}$ cm^3. L mol^{-1}, R_0 = 1.768 nm, *E* = 0.066 and *r* = 2.754 nm .From this

observation we found that donor-to-acceptor distance (*r)* between Trp residue at position 212 of BSA and complex is smaller than 7 nm, which indicates that energy transfer from BSA to complex. This result indicated that a static quenching interaction occurs between BSA and complex according to Forster's non radiative energy transfer theory.

Conformational changes (Synchronous fluorescence). During binding with complex the conformation of the BSA can alter which can be determined using synchronous fluorescence[92].According to the theory of Miller,[93] when the wavelength intervals ($\Delta\lambda$) value between the excitation and emission wavelengths are stabilized at 15 or 60 nm, the synchronous fluorescence spectra of the protein gives characteristic information about Tyr and Trp residues respectively and quenching of protein fluorescence caused by the ligand then implies alteration of the polarity around these residues. The effects of complex on the synchronous fluorescence spectra of BSA are shown in Fig.S17 in the Supporting Information (SI), when $\Delta\lambda$ fixed at 60nm the effect of complex on the synchronous fluorescence of BSA revealed that the fluorescence intensity diminished systematically with increasing concentration of the complex and large red shift of the emission maxima by 10 nm .A large red shift is indicative the change of Trp residues from a polar environment to a more hydrophilic environment and more exposed to solvent .Comparatively, there is small red(3nm) shift in the maximum emission wavelength using $\Delta\lambda$=15 showing that little transformation takes place in the microenvironment around tyrosines. Therefore upon interaction with complex microenvironments changes occur at Trp 212 which leads to the conclusion that Trp plays an important role during fluorescence quenching. This signified that complex approaches the Trp more than the Tyr which is good agreement with the results obtained from the FRET experiment.

Circular Dichroism (CD) studies. The change in secondary and tertiary structure of upon interaction with complex was monitored using Circular dichroism spectroscopy. Fig. 3C represents the CD spectra of BSA with increasing concentration of complex. From CD spectrum of native BSA showed two minima at 208 and 222 nm (curve 1) which is typical of α-helical structure[94,95] The 222 nm band corresponds to n→π∗ transition of the α-helix and the 222 nm band is due to π– π∗ transition for both the α-helix and random coil and are both contributed by the transition for the peptide bond of the α-helix. The secondary protein conformation, determined by the Jasco software, was found to contain 58.2.% α-helix, 23.4% β-sheet (both parallel and antiparallel) and 18.4% random coils, respectively, which is in close agreement with the literature reports. On binding with complex the CD maxima at 222 and 208 decrease regularly indicates a decrease of α-helical contain which is about 47.6%.From the CD spectra destabilization is clearly evident which is good agreement with the synchronous and FRET experiment.

Three-Dimensional fluorescence spectroscopy. Three dimensional fluorescence spectroscopy is another powerful technique to analyze the microenvironment and conformational changes in the protein on ligand binding on simultaneous change of excitation and emission wavelengths. The three-dimensional (3D) fluorescence spectra and the contour maps of the BSA and BSA in presence of complex are shown in Fig.6 resulting data collected in Supporting Information, Table S1. It exhibited four characteristic peaks; the peak a have been assigned as the first order Rayleigh scattering peak whose emission wavelength matches well with excitation wavelength (λem = λex) while the peak b as second order Rayleigh scattering peak (λem = 2λex). The interaction of BSA with complex leads to an increase in the diameter of the protein, which in turn results in the enhanced scattering effect. The peak 1 revealed spectral behavior of tyrosine

and tryptophan residues because the protein is excited at 280nm. In addition excitation at 230nm peak 2 is mainly caused by the $n \rightarrow \pi*$ transition and it is characteristics polypeptide backbone and secondary structure of the protein. These results showed that the fluorescence intensities of peak 1 exhibit significant stokes shift (10nm) and decrease in the intensity (61.1%). In case of peak2 there was no stokes shift but decrease in fluorescence intensity (21%). It further indicated that polarity of both the residues decreases, and new amino residues of BSA get buried into the hydrophobic pocket (Table S1 in the Supporting Information (SI)). Furthermore, decrease in the fluorescence intensity of peak 2) suggested extension of the polypeptide backbone to greater extent and BSA conformational changes[96]. Variation in Stokes shift and the decrease of fluorescence intensity of peaks 1 and 2 indicate that interaction between BSA and complex leads to changes in tyrosine and tryptophan residues, unfolding of the polypeptides residues, and conformation of the BSA.

Isothermal titration calorimetric studies.

ITC measurements provide detailed information on thermodynamic quantities discussed earlier and which can be correlated to the results of other experiments. In Fig. 4C representative calorimetric profiles of the titration of complex to BSA are presented. The binding is exothermic process in this case. The thermodynamic parameters obtained from the calorimetric studies are summarized in Table 4.The energetic of the binding of the complex was clearly enthalpy driven (ΔH = - 8.62± 0.40 kcal/mol) with a small entropy contribution ($T\Delta S$ = - 1.99 kcal/mol). The large value of enthalpy change is indicative of a stronger electrostatic interaction of complex. The binding constant of complex at 298.15 K was evaluated to be (7.26 ± 0.21) x 10^4 and The number of binding sites was (N=1.08).These values are quite close to the binding affinity values obtained from fluorescence titrations. On the other hand when the $Zn(ClO_4)_2.6H_2O$ titrated with

BSA yield a ΔH = -7.62± 0.40 kcal mol^{-1}, a stoichiometry (N) of 0.99 and K_b =(4.26 ± 0.11) x10^4 and the entropy contribution ($T\Delta S$) = -1.28 kcal/mole (Fig S14C and Table S2 in the Supporting Information (SI).) at 298.15K. From this comparative experiment it is quite clear that the binding of free Zn salt different from its complex.

Conclusions

In summary, the combination of our spectroscopic and calorimetric results of the synthesized complex revealed that the complex binds to the DNA and RNA duplex with a binding order 10^5 but the binding to CT-DNA is more exothermic with a unfavorable negative entropy change while the binding to Poly(I).Poly(C) was favored by negative enthalpy as well as positive entropy change. The binding mode of the complex to nucleic acids suggested from the EB displacement and circular dichriosm (CD) study that the mode probably by weak intercalation.

On the other hand interaction with BSA, formation of strong complex was revealed from absorbance and fluorescence quenching studies. The binding parameters calculated from Stern-Volmer quenching method revealed that the 10^4 order. Specific distance 'r' of 2.754 nm between Trp 212 of BSA and complex was obtained from Froster resonance energy transfer and was smaller than 7 nm, indicates that energy transfer from BSA to complex. Competitive binding using site marker having definite binding sites demonstrated that the binding site was site I (subdomain IIA) of BSA. The binding of the complex to BSA induced strong conformational changes as revealed from synchronous fluorescence, 3D fluorescence and circular dichroism studies. Thermodynamic parameters evaluated from isothermal titration calorimetry suggested that the binding was enthalpy driven and small negative entropy contributions.

The complex show evidence of binding with CT- DNA, double strand RNA(PolyI.PolyC) and BSA protein in an aqueous medium at physiological pH indicating the significance of designing

new water-soluble complex and can be used as potential binding agents to different biological macromolecules and subsequent metal-based drugs.

Acknowledgement

The project is financially supported by CSIR, New Delhi, India [No. 01(2536)/11/EMR-II] and UGC (New Delhi) [NO.F. 20 7(17)/2012(BSR)]. S.K.J is thankful to UGC for providing research fellowship. S.K.S is grateful to UGC (New Delhi) India, for financial support through MRP (42-830/2013 (SR)). We acknowledge support from the CIF facility of Bose Institute for CD experiments.

References

1. R.Martínez and L. Chacón-García,*Curr. Med. Chem.,*2005,**12,** 127-151.
2. H.K. Liu and J. P. Sadler, *Acc. Chem. Res.,*2011,**44,** 349-359.
3. W.A. Denny, *Curr. Med. Chem.,*2002,**9,** 1655-1665.
4. L.Strekowski and B. Wilson, *Mutat. Res.,*2007,**623,** 3-13.
5. V.Cepeda, M.A.Fuertes, J.Castilla, C.Alonso, C.Quevedo and J.M. Pérez,*Anticancer Agents Med. Chem.,*2007,**7**, 3-18.
6. R.P. Perez,*Eur. J. Cancer.,*1998,**34,** 1535-1542.
7. L.P.Martin, T.C.Hamilton and R.J. Schilder,*Clin. Cancer. Res.,*2008,**14,** 1291-1295.
8. V.Brabec and J. Kasparkova,*Drug. Resist. Updat.,*2005,**8,** 131-146.
9. E.R.Jamieson and S.J. Lippard,*Chem. Rev.,*1999,**99,** 2467-2498.
10. A.Łęczkowska and R. Vilar,*Annu. Rep. Prog. Chem. Sect. A: Inorg. Chem.,*2012,**108,** 330-349.

11. A.Łęczkowska and R. Vilar, R. *Annu. Rep. Prog. Chem. Sect. A: Inorg. Chem.,*2013,**109,** 299-316.

12. B.Nordén, P.Lincoln,B.Akerman and E. Tuite,*Met. Ions. Biol. Syst.,*1996,**33**, 177-252.

13. M.J.Clarke, F.Zhu and D.R. Frasca,*Chem. Rev.,*1999,**99**, 2511-2534.

14. D.Chen, V.Milacic, M.Frezza and Q.P. Dou,*Curr. Pharm. Des.,*2009,**15**, 777-791.

15. I.Ott and R. Gust,*Arch. Pharm. (Weinheim).,*2007,**340**, 117-126.

16. B.M.Zeglis, V.C. Pierre and J.K. Barton,*Chem. Commun.*, 2007,**28**, 4565-4579.

17. E. Meggers, *Chem. Commun.,*2009,**1**, 1001-1010.

18. U. Kragh-Hansen, *Pharmacol Rev.,*1981,**33,** 17-53.

19. B. P.Esposito and R.Najjar,*Coord. Chem. Rev.,*2002,**232**, 137-149.

20. A.Tarushi, X.Totta, A.Papadopoulos, J.Kljun, I.Turel, D.P.Kessissoglou and G. Psomas,*Eur. J. Med. Chem.,*2014,**74**, 187-198.

21. L. R. Gouvea, D. A. Martins, G. Batista Dda, N. Soeiro Mde, S. R. Louro, P. J. Barbeira, L. R. Teixeira, *Biometals.,* 2013,**26**, 813-825.

22. M.Anjomshoa, S.J.Fatemi, M.Torkzadeh-Mahani and H. Hadadzadeh,*Spectrochim. Acta A Mol. Biomol. Spectrosc.,*2014,**127**, 511-520.

23. M.Gharagozlou and D.M. Boghaei,*Spectrochim. Acta. A Mol. Biomol. Spectrosc.,*2008,**71**, 1617-1622.

24. C.Andreini, L.Banci, I.Bertini and A. Rosato,*J. Proteome., Res.*2006,**5**, 196-201.

25. H. Vahrenkamp,*Dalton Trans.*, 2007,**14,** 4751-4759.

26. H.Tapiero and K.D. Tew,*Biomed. Pharmacother.,*2003,**57**, 399-411.

27. W. Maret,*Biometals.,*2011,**24,** 411-418.

28. M.Di Vaira, C.Bazzicalupi, P.Orioli, L.Messori, B.Bruni and P. Zatta,*Inorg. Chem.,*2004,**43,** 3795-3797.

29. E.Ferrada, V.Arancibia, B.Loeb, E.Norambuena, C.Olea-Azarand J.P. Huidobro-Toro, *Neurotoxicology.,*2007,**28,** 445-449.

30. S.Emami, S.J.Hosseinimehr, S.M.Taghdisi and S. Akhlaghpoor,*Bioorg. Med. Chem. Lett.,*2007,**17**, 45-48.

31. Q.Huang, Z.Pan, P.Wang, Z.Chen, X.Zhang and H. Xu,*Bioorg. Med. Chem. Lett.,*2006,**16,** 3030-3033.

32. P.Lemoine, B.Viossat, N.H.Dung, A.Tomas, G.Morgant, F.T.Greenaway and J.R. Sorenson,*J. Inorg. Biochem.,*2004,**98,** 1734-1749.

33. J.d'Angelo, G.Morgant,N.E Ghermani, D.Desmaële, B.Fraisse, F.Bonhomme, E.Dichi, M.Sghaier, Y. Li, Y.Journaux and J. R. J. Sorenson, *Polyhedron.,*2008,**27,** 537-546.

34. Y.Yoshikawa and H. Yasui,*Curr. Top. Med. Chem.,*2012,**12,** 210-218.

35. H.Murakami, H.Yasui and Y. Yoshikawa,*Chem. Pharm. Bull. (Tokyo).,*2012,**60**, 1096-1104.

36. H.Sakurai, Y.Yoshikawa and H. Yasui,*Chem. Soc. Rev.,*2008,**37,** 2383-2392.

37. W.B.Júnior, M.S.Alexandre-Moreira, M.A.Alves, A.Perez-Rebolledo and G.L.Parrilha, E.E.Castellano, O.E.Piro, E.J.Barreiro, L.M.Lima and H. Beraldo,*Molecules.,*2011,**16,** 6902-6915.

38. A.Tarushi, X.Totta, C.P.Raptopoulou, V.Psycharis, G.Psomas and D.P. Kessissoglou,*Dalton Trans.,*2012,**41,** 7082-7091.

39. F.Zhang, Q.Y.Lin, W.L.Hu, W.J.Song, S.T.Shen and P. Gui,*Spectrochim. Acta A Mol. Biomol. Spectrosc.,*2013,**110,** 100-107.

40. P.F.Liguori, A.Valentini, M.Palma, A.Bellusci, S.Bernardini, M.Ghedini, M.L.Panno, C.Pettinari, F.Marchetti, A.Crispini and D.Pucci,*Dalton Trans.,*2010,**39,** 4202-4212.
41. B.Sanz Mendiguchia, D.Pucci, T.F.Mastropietro, M.Ghedini and A. Crispini,*Dalton Trans.,*2013,**42,** 6768-6774.
42. E. Kimura and M. Shionoya, *Met. Ions Biol. Syst.,*1996*,* **33,** 29-52.
43. S.Aoki and E.Kimura, *Chem. Rev.,*2004 *,* **104,** 769-787.
44. G.Barone, A.Terenzia, A.Lauriaa and A. M. Almericoa,*Coord. Chem. Rev.,*2013,**257,** 2848-2862.
45. R.J.Sundberg and R.B. Martin,*Chem. Rev.,*1974,**74,** 471-517.
46. H.Sigel and R.B. Martin,*Chem. Rev.,*1982,**82,** 385-426.
47. I.M.Pastor and M. Yus,*Curr. Chem. Biol.,*2009, **3,** 65-88.
48. N.Nagarajan, G.Vanitha, D.A.Ananth, A.Rameshkumar, T.Sivasudha and R. Renganathan,*J. Photochem. Photobiol. B.,*2013,**127,** 212-222.
49. Bruker, SAINT (Version 6.36a) Bruker AXS Inc., Madison, Wisconsin, USA, 2002.
50. Bruker, SMART (Version 5.625) and SADABS (Version 2.03a) Bruker AXS Inc., Madison, Wisconsin, USA, 2001.
51. G.M. Sheldrick,SHELXS97 and SHELXL97: Programs for Crystal Structure Solution and Refinement: University of Göttingen, Germany, 1997.
52. , L. J. Farrugia, *J. Appl. Crystallogr.,*1999,**32**, 837–838.
53. A.L.Spek, PLATON, A Multipurpose Crystallographic Tool: Utrecht University: Utrecht, The Netherlands, 2000.
54. A.Wolfe,G.H. Jr. Shimer and T. Meehan,*Biochemistry.,*1987,**26,** 6392-6396.

55. L.J. Farrugia,ORTEP III (Version 1.06) Department of Chemistry, University of Glasgow, Scotland, UK.

56. A.Tarushi, Z.Karaflou, J.Kljun, I.Turel, G.Psomas, A.N.Papadopoulos and D.P. Kessissoglou,*J. Inorg. Biochem.,*2013,**128,** 85-96.

57. F.Arjmand, A.Jamsheera and D.K. Mohapatra,*J. Photochem. Photobiol. B.*2013,**121,** 75-85.

58. A. Tarushi, K. Lafazanis, J. Kljun, I. Turel, A.A. Pantazaki, G. Psomas and D.P. Kessissoglou, *J. Inorg. Biochem.,* 2013, **121,** 53-65.

59. A. Zianna, G. Psomas, A. Hatzidimitriou, E. Coutouli-Argyropoulou and M. Lalia-Kantouri, *J. Inorg. Biochem*., 2013, **127,** 116.

60. I. Giannicchi, R. Brissos, D. Ramos, J. de Lapuente, J.C. Lima, A.D. Cort and L.Rodríguez, *Inorg. Chem.,*2013,**52,** 9245-9253.

61. E. Mrkalić, A. Zianna, G. Psomas, M. Gdaniec, A. Czapik, E. Coutouli-Argyropoulou and M. Lalia-Kantouri, *J. Inorg. Biochem*., 2014, **134,** 66.

62. J.B.LePecq and C. Paoletti,*J. Mol. Biol.,*1967,**27,** 87-106.

63. A.R.Morgan, J.S.Lee, D.E.Pulleyblank, N.L.Murray and D.H. Evans,*Nucleic Acids Res.,*1979,**7,** 547-569.

64. D.L.Boger, B.E.Fink, S.R.Brunette, W.C.Tse and M.P. Hedrick,*J. Am. Chem. Soc.,*2001,**123,** 5878-5891.

65. B.C.Baguley and M. Le Bret, *Biochemistry.,*1984,**23,** 937-943.

66. R.J.Douthart,J.P. Burnett,F.W.Beasley and B.H. Frank,*Biochemistry.,*1973,**12,** 214-220.

67. M.Vives, R.Gargallo and R. Tauler,*Anal. Chim. Acta.,*2000,**424**, 105-114.

68. E.Ramachandran, D.S.Raja, N.P.Rath and K. Natarajan,*Inorg. Chem.,*2013,**52,** 1504-1514.

69. A. Tarushi, E. Polatoglou, J. Kljun, Turel.; G. Psomas and D.P.Kessissoglou, *Dalton Trans.,*2011,**40,** 9461-9473.

70. A. Tarushi, C.P. Raptopoulou, V. Psycharis, A. Terzis, G.Psomas and D.P. Kessissoglou,*Bioorg. Med. Chem.,*2010,**18,** 2678-2685.

71. Y.M.Chang, C.K. M.Chen and M.H. Hou,*Int. J. Mol. Sci.,*2012,13, 3394-3413.

72. D.Hermann, C.Houssier, and W. Guschlbauer,*Biochimica. et Biophysica. Acta*., 1979,**564,** 456-472.

73. M.Vives,R. Gargallo,R.Tauler and V. Moreno,*J. Inorg. Biochem.,*2001,**85,** 279-290.

74. W. Chu, Y. Wang, S. Liu, X. Yang , S. Wang, S. Li,G. Zhou, X. Qin, C. Zhou and J. Zhang, *Bioorg. Med. Chem. Lett.,*2013,**23**, 5187-5191.

75. Y. Nakamura, Y. Taruno, M. Sugimoto, Y. Kitamura, H. L. Seng. S.M. Kong, C. H. Nge and M. Chikira. *Dalton Trans*., 2013, **42**, 3337-3345

76. J.B. Chaires,*Biopolymers.,*1997,**44,** 201-215.

77. J. R. Lakowicz,*Principles of fluorescence spectroscopy,* 3rd ed.; Springer: New York,2006.

78. Y.J. Hu, Y.Ou-Yang; C.M.Dai, Y.Liu and X.H. Xiao,*Biomacromolecules.,***2010**, *11*, 106-112.

79. D.S.Raja, N.S.Bhuvanesh and K. Natarajan,*Inorg. Chem.,*2011,**50,** 12852-12866.

80. T.Jr. Peters, *Adv. Protein. Chem.,*1985*,* **37,** 141-245

81. N.Tayeh, T.Rungassamy and J.R. Albani,*J. Pharm. Biomed. Anal.,*2009,**50,** 107-116.

82. J. R.Lakowicz, G .Freshwater and G. Weber,*Biophys. J.,*1980,**32,** 591-601.

83. J.R.Lakowicz and G. Weber,*Biochemistry.,*1973,**12,** 4161-4170.

84. J.R.Lakowicz and G. Weber,*Biochemistry.,*1973,**12,** 4171-4179.

85. G.Sudlow, D.J.Birkett and D.N. Wade,*Mol. Pharmacol.,*1976,**12,** 1052-1061.

86. G.Sudlow, D.J.Birkett and D.N. Wade,*Mol. Pharmacol.,*1975,**11,** 824-832.

87. S.Wanwimolruk, D.J.Birkett and P.M. Brooks,*Mol. Pharmacol.,*1983,**24,** 458-463.

88. L.Stryer and R.P. Haugland,*Proc. Natl. Acad. Sci. U S A.,*1967,**58,** 719-726.

89. T. Forster,*Ann. Phys.,*1948,**2,** 55-75.

90. B.Valeur and J.C. Brochon,*New trends in fluorescence spectroscopy*; Berlin: Springer, 1999.

91. B. Valeur,*Molecular Fluorescence: Principles and Applications*, Wiley VCH Verlag GmbH, 2001.

92. J. B. F. Lloyd, *Nat. Phys. Sci.,*1971,**231,** 64-65.

93. J. N. Miller,*Proc. Anal. Div. Chem. Soc.,*1979,**16,** 203-208.

94. R. W. Woody, Theory of Circular dichroism of Proteins, in *Circular Dichroism and the Conformational Analysis of Biomolecules*, Plenum Press Publisher, New York , 1996.

95. R.W. Woody,Circular dichroism. *Methods Enzymol.***1995***, 246*, 34-71.

96. J. Q.Tong, F.F.Tian, Q.Li, L.L.Li,C.Xiang,Y.Liu, J.Dai and F.L. Jiang,*Photochem. Photobiol. Sci.,*2012*,* **11,** 1868-1879.

Table 1 Crystal data and structure refinement parameters.

Structure	Zn^{II} Complex
Empirical formula	$C_{11}H_{13}N_4O_8Cl_1Zn_1$
Formula Weight	430.07
Temperature (K)	120(2)
Wavelength (Å)	0.71073
Crystal system	Monoclinic
space group	$P2_1/n$
a, b, c (Å)	13.6048(6), 6.5235(3), 19.0029(12)
α, β, γ (°)	90.00, 110.595(6), 90.00
Volume ($Å^3$)	1578.73(14)
Z / Density (calc.) (Mg/m^3)	4 / 1.809
Absorption coefficient (mm^{-1})	1.776
F(000)	872
Crystal size (mm^3)	0.42 × 0.25 × 0.19
θ range for data collection (°)	3.20 to 25.99
Limiting indices	-16<=h<=16, 7<=k<= -8, 23<=l<= -21
Reflections collected / unique	9906/3080 [R(int)=0.0329]
Completeness to θ (%)	99.3
Absorption correction	Semi-empirical from equivalents
Max. and min. transmission	0.996 and 0.993
Refinement method	Full-matrix least-squares on F^2
Data/parameters	3080 / 0 / 228
Goodness-of - fit on F^2	1.072
Final R indices [I > 2σ(I)]	R1=0.0305, *w*R2=0.0669
R indices (all data)	R1=0.0369, *w*R2=0.0705
Largest diff. peak and hole ($e.Å^{-3}$)	0.584 and -0.382

$R_1 = \sum||F_o|-|F_c||/\sum|F_o|$, $wR_2 = [\sum\{(F_o^2-F_c^2)^2\}/\sum\{w(F_o^2)^2\}]^{1/2}$, $w = 1/\{\sigma^2(F_o^2) + (aP)^2 + bP\}$, where a = 0.0246, b = 1.3195 and $P = (F_o^2 + 2F_c^2)/3$ for the structure.

Table 2 Hydrogen bonding geometry of the complex (Å, °).

D–H···A	d(D–H)	d(H···A)	d(D···A)	D–H···A	Symmetry
N13–H13···O2S	0.88	2.17	3.005(3)	158	2-x, 1-y, -z
N13–H13···O4S	0.88	2.57	3.243(3)	134	2-x, 1-y, -z
N23–H23···O1S	0.88	2.59	3.128(3)	120	1-x, 1-y, -z
N23–H23···O11	0.88	1.98	2.808(3)	157	1-x, 1-y, -z
C1–H1···O2	0.95	2.56	3.132(3)	119	3/2-x, -1/2+y, 1/2-z
C16–H16C···O21	0.98	2.48	3.383(3)	152	2-x, 1-y, -z
C17–H17···O21	0.95	2.44	3.345(3)	159	x, 1+y, z
C22–H22···O3S	0.95	2.38	3.310(3)	168	1-x, 1-y, -z

Table 3 Geometrical parameters (Å, º) for the π-stacking moieties involved in the π···π interactions for the title complex.

rings *i-j*	Rc[a]	R1v[b]	R2v[c]	α[d]	β[e]	γ[f]	Symmetry
Cg(4)···Cg(4)	3.4690(15)	3.2558(10)	3.2558(10)	0.00	20.20	20.20	1-x, -y, -z
Cg(4)···Cg(4)	3.7278(15)	3.2123(10)	3.2122(10)	0.00	30.49	30.49	1-x, 1-y, -z

Cg(4) is the centroids of the (N21/C22/N23/C24/C25) ring. [a]Centroid distance between ring i and ring j. [b]Vertical distance from ring centroid i to ring j. [c]Vertical distance from ring centroid j to ring i. [d] Dihedral angle between the first ring mean plane and the second ring mean plane of the partner molecule. [e]Angle between centroids of first ring and second ring mean planes. [f] Angle between the centroid of the first ring and the normal to the second ring mean plane of the partner molecule.

Table 4 ITC derived thermodynamic parameters for the binding of Zn complex to CT-DNA, RNA and BSA in CP buffer of 10mM [Na^+], pH 7.01 [a]

	Temperature (K)	Binding constant (K_b) M^{-1}	Stoichiometry (N)	ΔG (kca/mol)	ΔH (kca/mol)	$T\Delta S$ (kca/mol)
CT-DNA	298.15	(1.8 ± 0.39) x10^5	0.359±0.0191	-7.17±1.90	-53.69±1.90	-46.51
RNA(polyI.polyC)	298.15	(2.81±0.17) x10^5	0.390±0.004	-7.44 ± 0.03	-3.09 ± 0.03	4.35
BSA	298.15	(7.26±0.21) x10^4	1.08±0.15	-6.63± 0.40	-8.62± 0.40	-1.99

[a] Average from two determinations each. All ITC profiles fit to a model of single binding sites.

Table 5 Variation of the binding constant of complex to BSA in presence of site markers of derived from the Stern-Volmer method at 30 ^{O}C

Site marker	K_a /10^{-4} L.mol^{-1}
Blank	3.74
Ibuprofen	2.29
Warfarin	1.28

Figure and legends:

Fig. 1 ORTEP view and atom numbering scheme for the title structure. The displacement thermal ellipsoids are drawn at 30% probability level.

Fig. 2 Absorption spectral changes of (A) Zn complex (5μM) treated with 0, 5, 10, 15, 20 and 25 μM (curves 1–6) of CT-DNA and (B) Zn complex (5μM) treated with 0, 5, 10, 15, 20 ,25 and 30 μM (curves 1–7) of RNA (PolyI.PolyC). Inset: shows a fitting of the absorbance data used to obtain the binding constants.

Fig. 3 Intrinsic circular dichroic (far UV) spectral changes of (A) CT-DNA (30 μM), (B) RNA(PolyI.PolyC) (30 μM) and (C) BSA(1 μM). In panel (A) curves 1 to 5 denote 0, 15, 30, 45, and 60 μM of Zn complex, panel (B) curves 1 to 5 denote 0, 15, 30, 45, and 60 μM of Zn complex and panel (C) curves 1 to 5 denote 0, 5, 10, 15 and 20 μM of Zn complex.

Fig. 4 ITC profiles for the binding of Zn complex to (A) CT-DNA, (B) RNA (PolyC.PolyI) and (C) BSA. Top panels present raw results for the sequential injection of (A) CT-DNA, (B) RNA (PolyC.PolyI) , (C) BSA in citrate-phosphate buffer, pH 7.01 at 25 ^{o}C and the respective dilution controls (curves on the top off set for clarity).The bottom panels show the integrated heat results after correction of heat of dilution against the mole ratio. The data points were fitted to one site model and the solid lines represent the best-fit data.

Fig. 5 Fluorescence spectra of BSA (5μM) (T=30^{o}C, λ_{ex}=295 nm) treated with different concentrations of (A) Zn complex. In panel (A) curves (1-7) denote 0, 2, 4, 8, 12, 16, 18 and 25 μM of Zn complex. Effect of site marker on the Zn complex-BSA system (T= T=30^{o}C, λ_{ex}=295 nm) in (B) c (warfarin)= c (BSA)= 5μM and (C) c (ibuprofen)=c (BSA)=5μM respectively. In panel (B) curves (1-7) corresponds to 0, 2, 4, 8, 12, 16, 18 and 25 μM of Zn complex. and panel (c) curves (1-7) denote 0, 2, 4, 8, 12, 16, 18 and 25 μM of Zn complex. Panel (D) Stern-Volmer plots of Zn complex and site marker competitive experiments, blank (■), in presence of warfarin (▲) and in presence of ibuprofen (•).

Fig. 6 Three-dimensional contour and fluorescence spectra of BSA 2.5 μM (A, C) and 1:10 BSA+Zn complex (B, D)

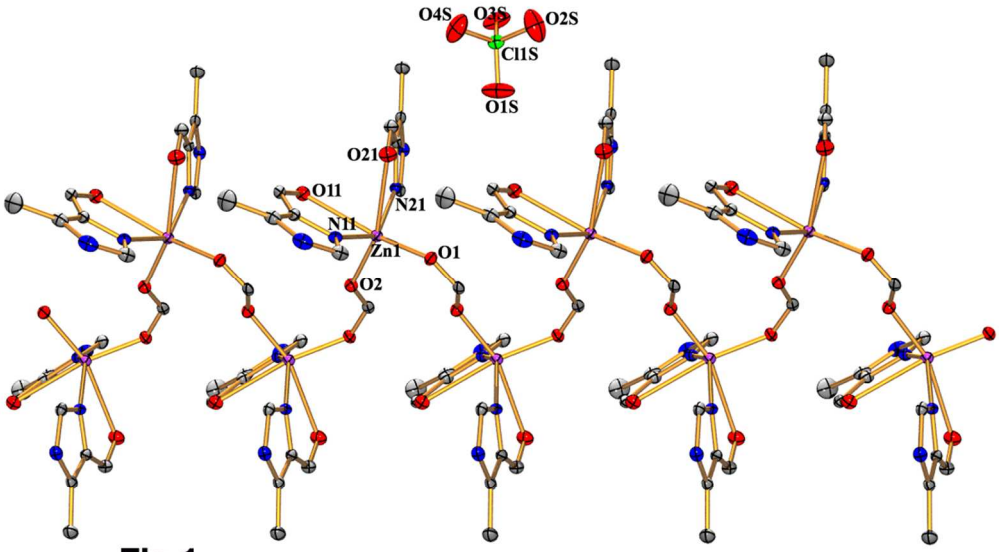

Fig.1

ORTEP view and atom numbering scheme for the title structure. The displacement thermal ellipsoids are drawn at 30% probability level.
101x63mm (300 x 300 DPI)

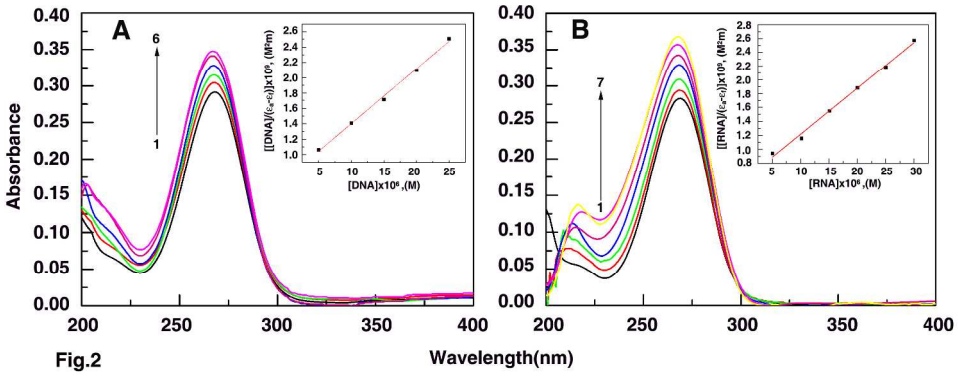

Fig.2

Absorption spectral changes of (A) Zn complex (5μM) treated with 0, 5, 10, 15, 20 and 25 μM (curves 1–6) of CT-DNA and (B) Zn complex (5μM) treated with 0, 5, 10, 15, 20 ,25 and 30 μM (curves 1–7) of RNA (PolyI.PolyC). Inset: shows a fitting of the absorbance data used to obtain the binding constants.
266x108mm (300 x 300 DPI)

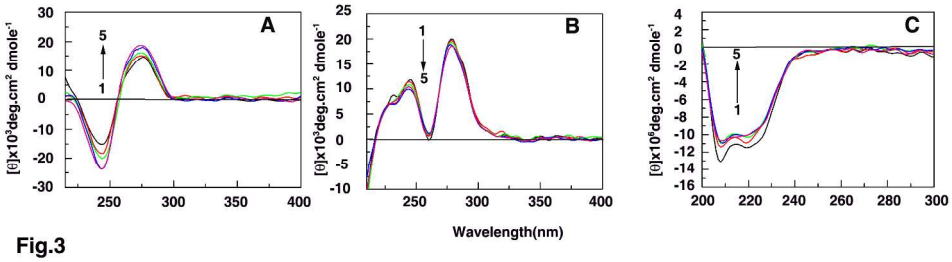

Fig.3

Intrinsic circular dichroic (far UV) spectral changes of (A) CT-DNA (30 μM), (B) RNA(PolyI.PolyC) (30 μM) and (C) BSA(1 μM). In panel (A) curves 1 to 5 denote 0, 15, 30, 45, and 60 μM of Zn complex, panel (B) curves 1 to 5 denote 0, 15, 30, 45, and 60 μM of Zn complex and panel (C) curves 1 to 5 denote 0, 5, 10, 15 and 20 μM of Zn complex.
247x76mm (300 x 300 DPI)

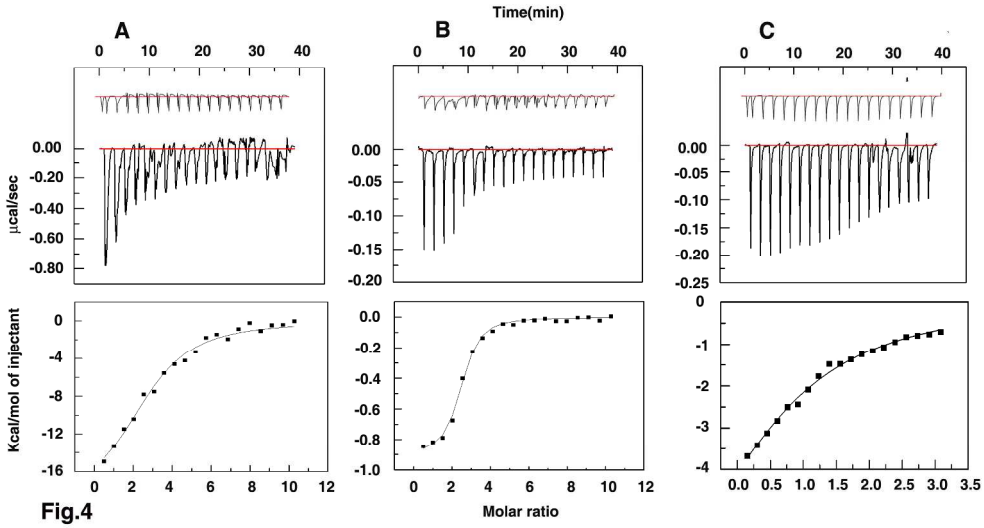

Fig.4

ITC profiles for the binding of Zn complex to (A) CT-DNA, (B) RNA (PolyC.PolyI) and (C) BSA. Top panels present raw results for the sequential injection of (A) CT-DNA, (B) RNA (PolyC.PolyI) , (C) BSA in citrate-phosphate buffer, pH 7.01 at 25 oC and the respective dilution controls (curves on the top off set for clarity).The bottom panels show the integrated heat results after correction of heat of dilution against the mole ratio. The data points were fitted to one site model and the solid lines represent the best-fit data.
236x134mm (300 x 300 DPI)

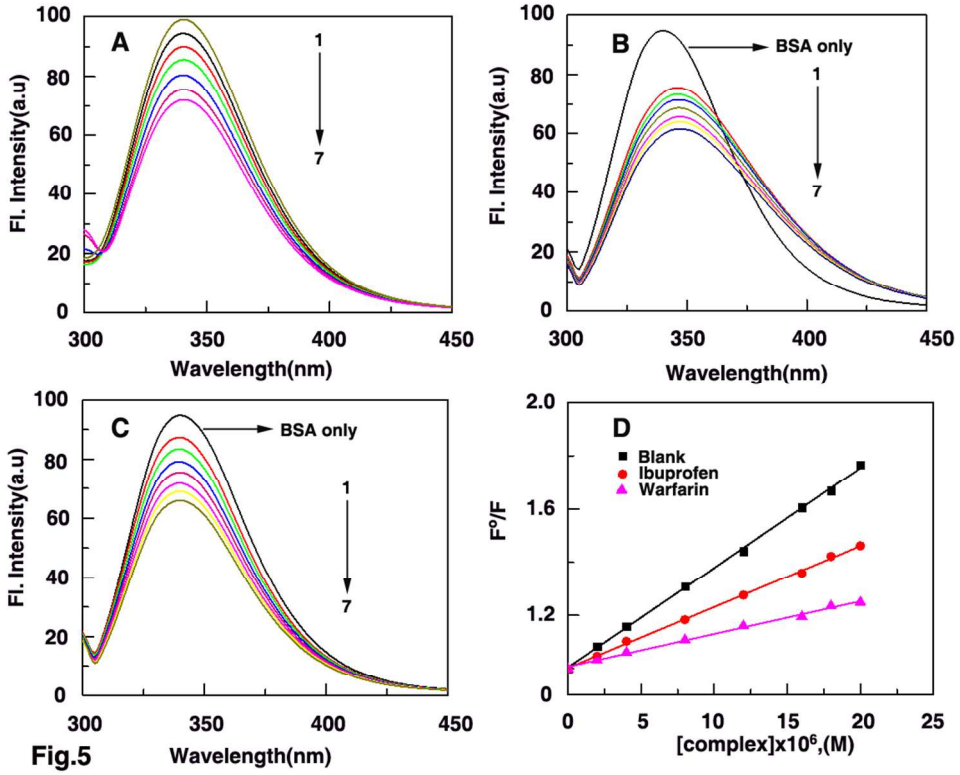

Fig.5

Fluorescence spectra of BSA (5μM) (T=30oC, λex=295 nm) treated with different concentrations of (A) Zn complex. In panel (A) curves (1-7) denote 0, 2, 4, 8, 12, 16, 18 and 25 μM of Zn complex. Effect of site marker on the Zn complex-BSA system (T= T=30oC, λex=295 nm) in (B) c (warfarin)= c (BSA)= 5μM and (C) c (ibuprofen)=c (BSA)=5μM respectively. In panel (B) curves (1-7) corresponds to 0, 2, 4, 8, 12, 16, 18 and 25 μM of Zn complex. and panel (c) curves (1-7) denote 0, 2, 4, 8, 12, 16, 18 and 25 μM of Zn complex. Panel (D) Stern-Volmer plots of Zn complex and site marker competitive experiments, blank (■), in presence of warfarin (△) and in presence of ibuprofen (•).
203x158mm (150 x 150 DPI)

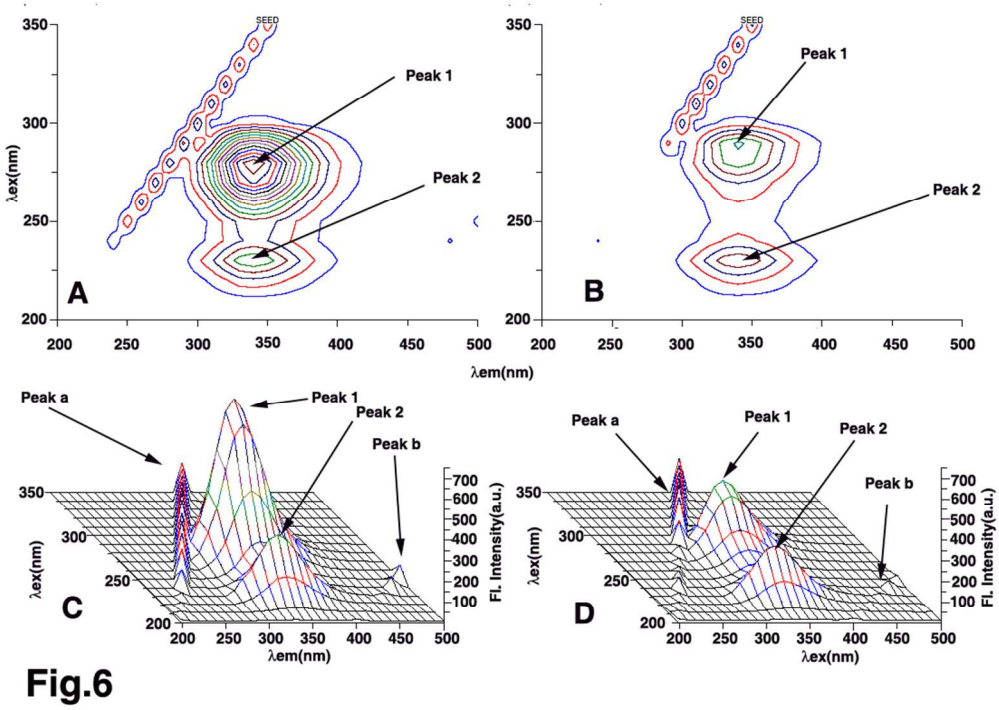

Fig.6

Three-dimensional contour and fluorescence spectra of BSA 2.5 μM (A, C) and 1:10 BSA+Zn complex (B, D)
93x66mm (300 x 300 DPI)